



Synthesis of Reduced Graphene Oxide-Silver Nanocomposites and Assessing Their Toxicity on the Green Microalga *Chlorella vulgaris*

Fatemeh Nazari¹ · Ali Movafeghi¹ · Saeed Jafarirad² · Morteza Kosari-Nasab³ · Baharak Divband⁴

Published online: 15 September 2018
© Springer Science+Business Media, LLC, part of Springer Nature 2018

Abstract

The growing demands for nanotechnology in the recent years have resulted in environmental release of nanomaterials. In the current study, reduced graphene oxide-silver nanocomposites (Ag-rGO) were synthesized by an easy method and their characteristics were determined using X-ray diffraction (XRD), ultraviolet-visible spectroscopy (UV-Vis), energy dispersive X-ray spectroscopy (EDX), and scanning electron microscopy (SEM) techniques. Subsequently, toxicity of Ag-rGO was examined on the marine microalga *Chlorella vulgaris*. After treatment of algal cells with different concentrations of Ag-rGO for 24 h, growth parameters have been significantly decreased. In addition, a considerable reduction in viability of the treated cells was designated. Further considerable effects of Ag-rGO treatments have been revealed by increments in the activities of a number of antioxidant enzymes and reductions in the photosynthetic pigment contents. Our results showed that the main toxic effects of Ag-rGO are associated with the presence of Ag nanoparticles in the structure of these nanocomposites.

Keywords Ag-rGO nanocomposites · *Chlorella vulgaris* · Green microalga · Toxicity · Oxidative stress

1 Introduction

Graphene is a two-dimensional and one-atom-thick sheet that is formed of monolayers of carbon atoms organized in a honeycombed network containing six-membered rings [1]. Because of its exceptional electronic and mechanical properties, excessive mobility of charge carriers, specific magnetism, and noteworthy thermal conductivity, graphene has attracted a lot of attention in various scientific and industrial areas [2]. Graphene oxide (GO) is an oxidized derivative of graphene, which has oxygen-containing groups including epoxy, hydroxyl, and carboxyl. As one of the most major graphene-derived materials, GO exhibits outstanding electrochemical

properties and has promising applications in numerous fields such as biotechnology and electronics [3]. GO can act as the platform for growing and immobilization of metal nanoparticles. Accordingly, GO and its composites have a wide range of potential utilizations on transistors, polymer reinforcement transparent conductors, biomaterials, and bioengineering fields [4]. However, harmful effects of GO on organisms have been indicated by both in vitro and in vivo analyses. Investigations of cell lines and animal species have confirmed the distribution and translocation of GO in living organisms [5].

High catalytic activity of silver (Ag) for quite a lot of chemical reactions, including dissociation of ozone, reduction of NO_x, ethylene and propylene epoxidation, and reduction of nitrophenols, has attracted increasing attention. High surface energy of nanoparticles leads to their thermodynamic instability and aggregation, which resulted in a gradual elimination of the catalytic efficiency of the nanoparticles. GO is one of the suitable support substrates that is used for the development and stabilization of Ag nanoparticles in order to generate high-performance Ag nanoparticle-based catalysts such as reduced graphene oxide-silver nanocomposites (Ag-rGO) [6].

Algae as primary producers play a main role in the aquatic ecosystems by providing oxygen and organics for other organisms [7]. Microalgae are widespread in lakes

✉ Ali Movafeghi
movafeghi@tabrizu.ac.ir

¹ Department of Plant Biology, Faculty of Natural Sciences, University of Tabriz, Tabriz, Iran

² Research Institute for Fundamental Sciences (RIFS), University of Tabriz, Tabriz, Iran

³ Drug Applied Research Center, Tabriz University of Medical Sciences, Tabriz, Iran

⁴ Dental and Periodontal Research Center, Tabriz University of Medical Sciences, Tabriz, Iran

and seas, easy to culture and propagate, and susceptible to pollutants. Therefore, they are one of normally utilized aquatic models for the toxicity assessment of toxicants and nanomaterials as well [8].

Chlorella vulgaris is a unicellular green microalga with typical structure of plant cells and is one of the established bioindicators for exploring the toxicity of nanomaterials [9]. In consequence of various industrial applications of Ag-rGO and their release to the environment, studying the toxicity of this nanocomposite on *C. vulgaris* as a model photosynthetic alga is highly needed. The findings of this investigation may shed light on the potential toxic impacts of Ag-rGO on other living organisms. Nanomaterials have unique chemical and physical features in comparison with their bulk forms because of their size at the nanoscale [10, 11]. Different responses have been observed in microalgae exposed to nanomaterials, including growth inhibition, reduction in the amount of photosynthetic pigments, and induction of oxidative stress [9, 12, 13]. The main objectives of the current study were to investigate the toxicological effects of Ag-rGO on *C. vulgaris* by utilizing a growth inhibition test and examination the underlying mechanisms of Ag-rGO toxicity. Separately, the effects of GO were also considered at the same concentrations to show that the main toxic effects of Ag-rGO are associated to the presence of Ag nanoparticles in its structure. After treatments with different concentrations of Ag-rGO and GO, growth parameters, content of photosynthetic pigments, antioxidant enzymes activities, cell viability, and morphology of the algae were analyzed.

2 Materials and Methods

2.1 Synthesis of GO and Ag-rGO

GO was prepared by a modified Hummer procedure [14]. By using 50 g of NaCl, 1 g of graphite was pulverized for 10 min. Subsequently, NaCl was dissolved and eliminated through filtration. The ground graphite was stirred in 23 mL of 98% H₂SO₄ for a period of 20 h. In the next step, 3 g of KMnO₄ was gradually added while stirring at a temperature less than 20 °C. The mixture was stirred at 40 °C and 80 °C for 30 and 45 min, respectively. After adding 46 mL of deionized water, the temperature was increased to 100 °C for 30 min. At the end, 140 mL of deionized water and 10 mL of 30% H₂O₂ solution were added. After washing with 5% HCl solution and then with deionized water, the final product was dried.

For green synthesis of Ag-rGO, 0.1 g synthesized GO was mixed in 8 mL of deionized water and placed in an ultrasonic bath for 1 h to get homogenous dispersion. After that, 0.056 M silver nitrate solution was gradually added to the GO suspension. The reaction mixtures were put in an ultrasonic bath for

3 h and then kept under vigorous stirring for 24 h at 40 °C. Subsequently, 20 mL of *Hibiscus sabdariffa* extract were prepared according to the method reported by [15] and were added to the suspension of Ag-GO. After vigorous stirring for 3 h at 80–90 °C, obtained solution was centrifuged and solid sediment was dried after repeated washing with deionized water.

2.2 Characterization of Prepared GO and Ag-rGO

The crystalline phase of GO and Ag-rGO was determined by X-ray diffraction (PANalytical X'Pert PRO-Germany) Cu-K_α radiations ($\lambda = 1.54 \text{ \AA}$). In addition, size and shape determination of the nanomaterials was carried out using scanning electron microscopy (MIRA3 FEG-SEM). Energy dispersive X-ray analysis (EDX) coupled to FESEM was used for the elemental analysis of nanomaterials. The Raman spectroscopy (Takram P50C0R10-Teksan) with a 532-nm laser was utilized to analyze Ag-rGO structure. UV-Vis absorption spectra of the GO and Ag-rGO were obtained by a spectrophotometer (Analytik Jena, Specord 250).

2.3 Cultivation of Algal Cells

C. vulgaris was cultured in 1-L Erlenmeyer flasks containing BG-11 medium. Sterilizing the culture medium and Erlenmeyer flasks was done in an autoclave at 121 °C for 20 min. The media were inoculated with *C. vulgaris* cells and the algae were grown for 5–7 days with consecutive aeration. The cultures were kept at 25 °C under a 16:8-h light:dark regime. The cell density was monitored spectrophotometrically at 680 nm every 24 h using a spectrophotometer combined with a hemocytometer. The regression equation for the correlation of cell density ($y \times 10^6 \text{ cells mL}^{-1}$) with absorption at 680 nm (x) was computed as $y = 7.0988x - 0.4298$ ($p < 0.05$, $R^2 = 0.9555$).

2.4 Scanning Electron Microscopy of Cells

After 24 h of exposure to GO and Ag-rGO (30 mg/L), the morphology of treated and untreated algal cells was assessed by scanning electron microscopy. Aliquots of algal cells were centrifuged and subsequently the algal cells were washed by adding BG-11 medium to the algal pellets. After centrifugation, the samples were kept at $-20 \text{ }^\circ\text{C}$ for 24 h and then were freeze-dried for 1 h. After subjecting to gold sputtering, freeze-dried cells were observed using a SEM (MIRA3 FEG-SEM).

2.5 Flow Cytometric Analysis

After centrifugation, algal cells were washed using phosphate buffer solution (PBS), and propidium iodide (PI) was

utilized for staining the cells. After a time period of 30 min, the emitted fluorescence of PI was gathered in the BD FACSCalibur FL2 channel [16].

2.6 Determination of Antioxidant Enzymes' Activities

The algal cells were harvested by centrifugation and were homogenized in liquid N₂. Then, the algal pellets were homogenized again in 0.05 M phosphate buffer (pH 7.0) at 4 °C. After centrifugation, the supernatant was used for assessment of the activity of antioxidant enzymes. The Bradford reagent and bovine serum albumin (BSA) were used as standard for determination of protein concentration [17].

The activity of catalase (CAT, EC 1.11.1.6) was measured by recording the decrease in absorbance of H₂O₂ at 240 nm and decomposition of 1 μmol of H₂O₂/min was considered as one unit of enzyme activity [18]. Ascorbate peroxidase (APX, EC 1.11.1.11) activity was determined using the method reported by Boominathan and Doran [19]. Oxidation of ascorbic acid was followed as a reduction in absorbance at 290 nm. The amount of protein required for the oxidation of 1 μmol ascorbic acid/min was defined as one unit of enzyme activity. The activity of superoxide dismutase (SOD) was measured by tetrazolium reduction procedure [20]. One unit of SOD was considered as the amount of enzyme inhibiting 50% of nitro blue tetrazolium (NBT) reduction under the specified conditions. The alteration in absorbance was recorded at 560 nm.

2.7 Quantification of Photosynthetic Pigments

C. vulgaris cells were first centrifuged and then the pellets were homogenized in absolute methanol. The absorbance of the methanolic extract was measured at the wavelengths of 470, 653, and 665 nm by a spectrophotometer. The contents of chlorophylls and carotenoids of the extract were computed using the equations reported by [21]:

$$C_a = 15.65A_{665} - 7.340A_{653}$$

$$C_b = 27.5A_{653} - 11.21A_{665}$$

$$C_{x+c} = 1000A_{470} - 2.860C_a - 129.2C_b/245$$

2.8 Statistical Analysis

The experimental assessments of this study consisted of three replicates. Statistical significant differences between groups were determined using analysis of variance (ANOVA) test with the statistical software SPSS 22.0. Statistical significance was considered at *p* values less than 0.05.

3 Results and Discussion

3.1 Characteristics of Ag-rGO and GO

The XRD spectra of synthesized GO and Ag-rGO are given in Fig. 1. Accordingly, GO indicates an intensive peak at 11° (Fig. 1a) and Ag-rGO possesses the combined structure of rGO and Ag nanoparticles (Fig. 1b). The appeared peak at 25.8° relates to the rGO. The diffraction peaks at 27.92°, 32.37°, 38.26°, 46.37°, 64.61°, and 77.52° correspond to the reflection of (210), (122), (111), (231), (220), and (311) planes of Ag nanoparticles phase, respectively. These diffraction patterns belong to face-centered cubic silver [15]. SEM images of GO and Ag-rGO are also presented in Fig. 1. As indicated in Fig. 1c, synthesized GO has a flaky morphology. According to Fig. 1d, Ag-rGO has been composed of GO sheets deposited by a great density of spherical Ag nanoparticles. The details of elements existing in the Ag-rGO were presented by EDX analysis in weight percentage (Fig. 2a). Ag-rGO was formed of carbon (56.08%), oxygen (13.15%), and silver (30.77%). The existence of silver, carbon, and oxygen verifies the formation of Ag-rGO nanocomposites. The formation of GO and Ag-rGO was also established by UV-Vis absorption spectra (Fig. 2b). The UV-Vis spectrum of GO indicated a maximum band at 239 nm and a shoulder band at about 300 nm. The bands of UV-Vis spectrum of Ag-rGO at 257 nm and 392 nm belong to the rGO and Ag nanoparticles, respectively [22, 23]. Due to its non-ruinous feature, the Raman spectroscopy is a widely utilized analysis for determination of graphene-related materials. The Raman spectrum of Ag-rGO indicates two outstanding peaks at 1349 and 1566 cm⁻¹ (Fig. 2c), which belong to the well-evidenced G and D bands [6].

3.2 Assessing the Growth of *C. vulgaris*

Cell numbers were recorded at different concentrations of Ag-rGO and GO after 6, 18, and 24 h of exposure. Subsequent to the treatment with Ag-rGO (10, 20, and 30 mg/L), cell numbers have been significantly decreased compared to the control (Fig. 3a). The low Ag-rGO concentration (1 mg/L) had no significant effect on cell quantities. After treatment of the algal cells with GO (1, 10, 20, and 30 mg/L), cell numbers have been slightly decreased compared to the untreated control (Fig. 3b). Thus, Ag-rGO was found to be more toxic to the cells, because cell numbers reduced stronger compared to GO.

Figure 4 indicates the results of Ag-rGO and GO effects on fresh and dry weight after 24 h of treatment. Compared to the control, Ag-rGO has caused a decrease in both fresh weight (at the concentrations of 1, 10, 20, and 30 mg/L) and dry weight (at the concentrations of 20 and 30 mg/L). On the other hand, no significant difference was found among the concentrations of 1 and 10 mg/L of GO compared to the control. GO treatment had no considerable effect on dry weight. The inhibition

Fig. 1 X-ray diffraction (XRD) patterns of GO (a) and Ag-rGO (b), and scanning electron microscope (SEM) images of GO (c) and Ag-rGO (d)

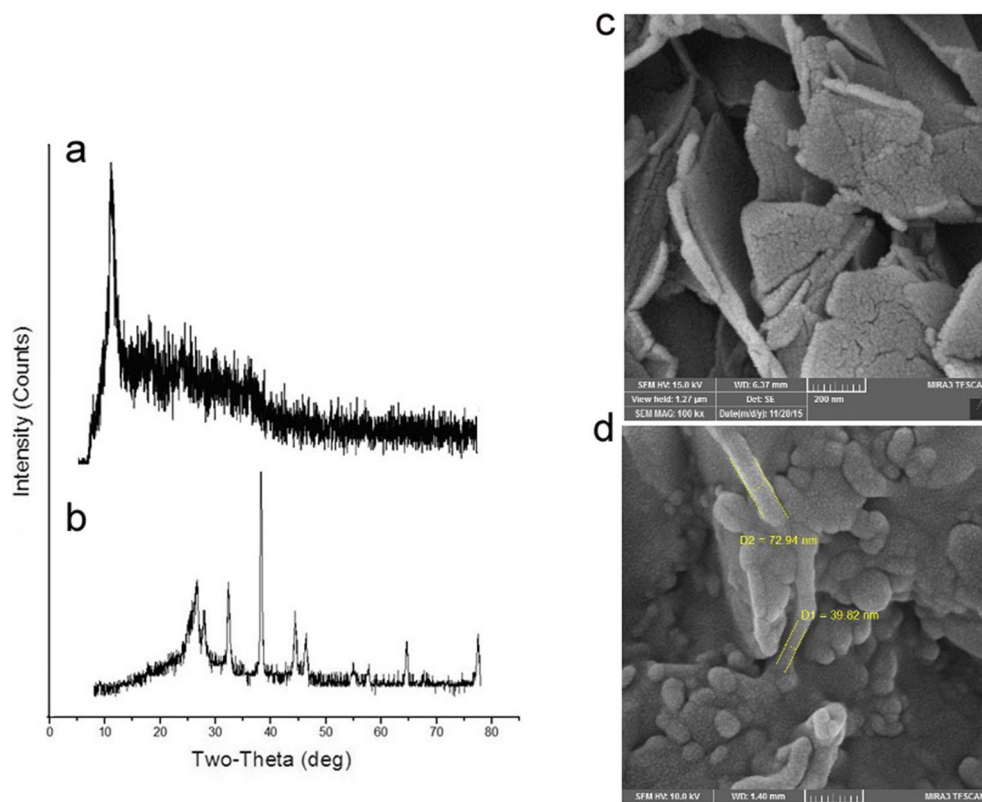
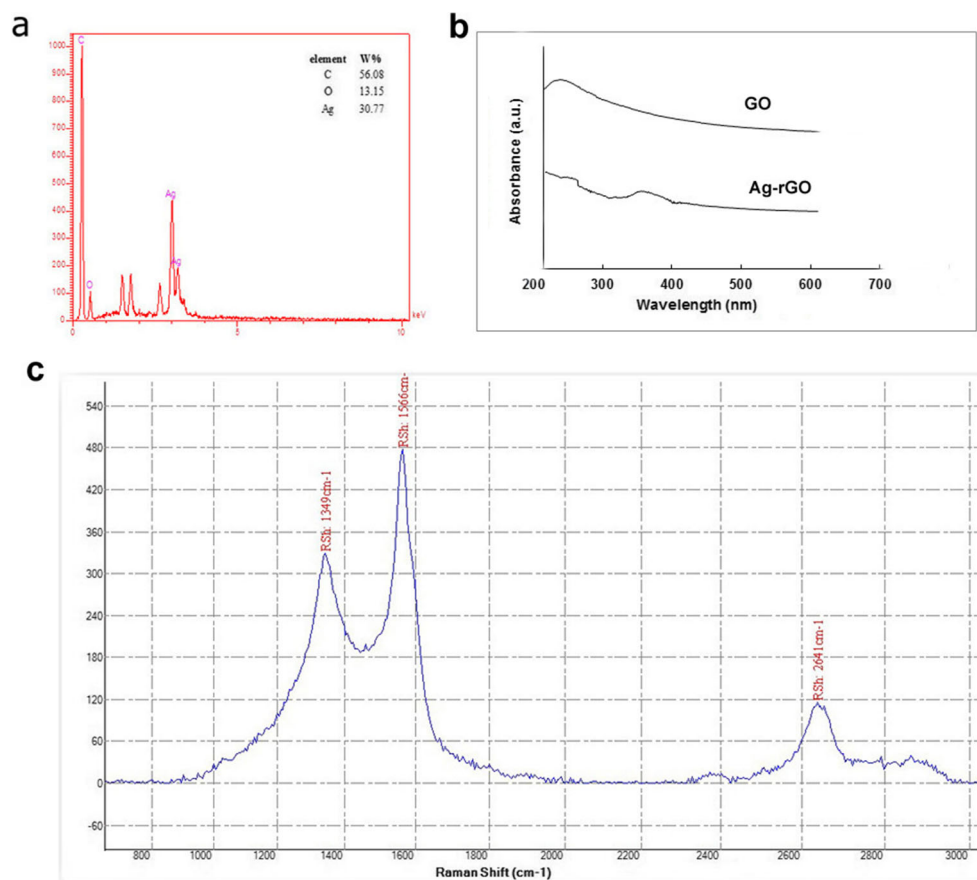


Fig. 2 Energy dispersive X-ray analysis (EDX) of Ag-rGO (a), UV-Vis spectra of GO and Ag-rGO (b) and the Raman spectrum of Ag-rGO (c)



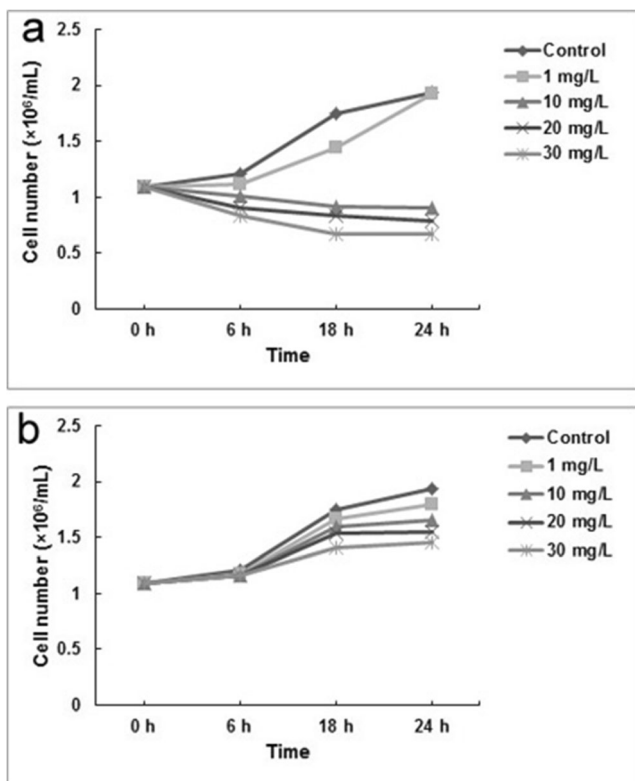


Fig. 3 The effects of Ag-rGO (a) and GO (b) on algal cell number as growth parameter after 6, 18, and 24 h of exposure

of the growth of *C. vulgaris* by ZnO and NiO nanoparticles has also been formerly reported [24, 25]. Additionally, Ag nanoparticles have described to possess a potential for inducing toxicity in *C. vulgaris* [26]. Our results revealed that the occurrence of Ag nanoparticles in the structure of Ag-rGO is the main reason for the growth reduction of algal cells.

3.3 Morphology of the Treated Cells

According to the SEM images (Fig. 5), there were no obvious differences in cellular morphology between the control and GO-treated cells (30 mg/L) after 24 h of exposure. In comparison, Ag-rGO (30 mg/L) has induced an intensive shriveled and dried up morphology. These findings are in fair agreements with previous reports establishing changes in the shapes and sizes of different algal species under toxic nanoparticle exposure [16, 27].

3.4 Assessment of Cell Viability by Flow Cytometry

Flow cytometric analysis was used for determining the cytotoxicity levels in algal cells. By the death of cell, the loss of membrane integrity occurs and red fluorescent nucleic acid dye PI can pass the membranes and stain the nucleic acids [16]. In flow cytometry diagrams, upper left and right quadrants represent the amount of dead cells and lower left and

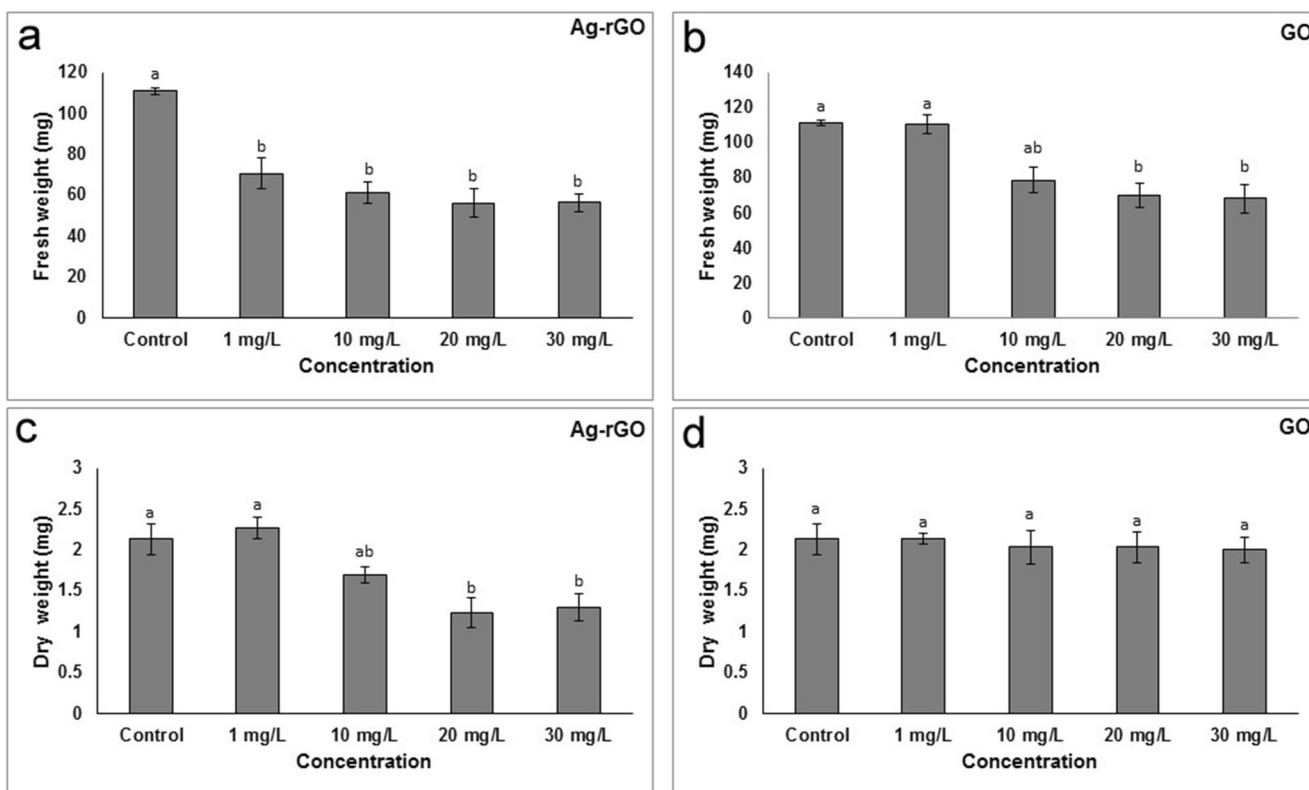
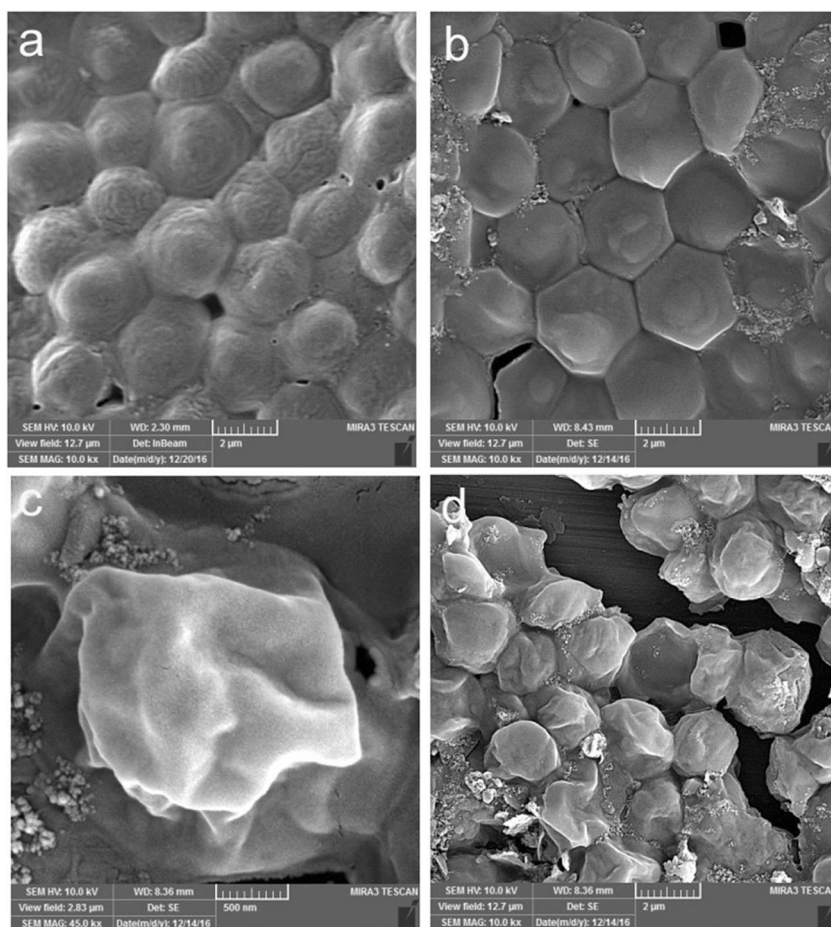


Fig. 4 The effects of Ag-rGO (a, c) and GO (b, d) on fresh and dry weight of *C. vulgaris* cells after 24 h of exposure. Different letters indicate significant differences at $p < 0.05$. The error bars show standard deviation of the mean ($n = 3$ replicates)

Fig. 5 Scanning electron microscope (SEM) images of cells of control (**a**), GO-treated (**b**), and Ag-rGO-treated (**c, d**) *C. vulgaris* after 24 h of exposure



right quadrants demonstrate the proportion of living cells. The percentage of viable cells for the control sample was approximately 100% after 24 h (Fig. 6a). In comparison, the cell viability was reduced to 57.82% after treatment with Ag-rGO at the concentration of 30 mg/L (Fig. 6b). Intriguingly, the cell viability was verified by 98.82% for GO treatment (Fig. 6c). These data are in agreement with the obtained results of scanning electron microscopy analysis confirming the toxic impacts of Ag-rGO on the algal cells.

3.5 Activities of Antioxidant Enzymes

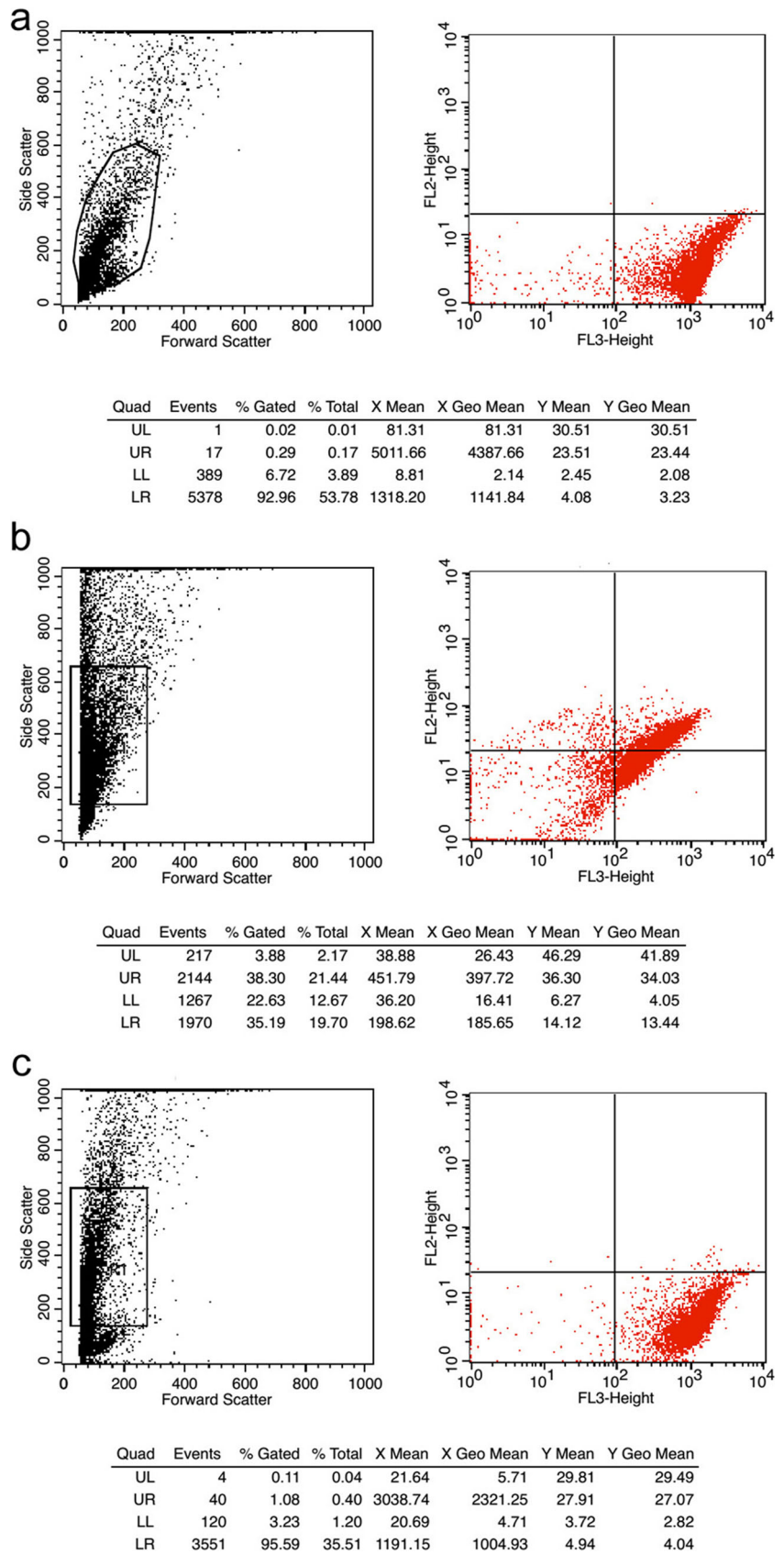
Ag-rGO at the concentrations of 1 and 10 mg/L slightly and at 20 and 30 mg/L significantly enhanced the activities of SOD and APX in comparison with the control (Fig. 7a, c, respectively). Slight stimulation of SOD and APX activities was also observed after GO treatment (Fig. 7b, d, respectively); however, there were no significant differences in SOD and APX activities between the control and GO-treated cells. A concentration-dependent reduction in the CAT activity was obvious in the cells of *C. vulgaris* exposed to Ag-rGO (Fig. 7e). The results indicated no evident effect on CAT activity for GO treatment (Fig. 7f).

Plants have been shown to use different antioxidant enzymes or low molecular weight antioxidants to manage ROS levels [28]. SOD can be considered as a key enzyme in the elimination of ROS. SOD, as a fundamental component of antioxidative defense system in plants, has the responsibility of converting superoxide radicals to H_2O_2 with high speed [29]. An enhanced activity of SOD is in good agreement with the previous reports [28, 30, 31]. The Ag-rGO-mediated increment in capability of SOD, found in this research, may be obtained due to either direct effect of the nanomaterial on the SOD gene or to an indirect effect mediated by an enhancement in the content of O_2^- radicals [29, 32].

APX as an essential component of the ascorbate/glutathione pathway is needed to scavenge H_2O_2 and is usually generated in chloroplast and other organelles to retain the redox state of the cell. The high affinity of APX for H_2O_2 allows the scavenging of low quantity of H_2O_2 in more special locations [29]. Increased activity of APX is similar to the results obtained by [29] at low concentrations. The stimulated activity of APX by Ag-rGO in *C. vulgaris* suggested direct active role of antioxidants in detoxifying oxygen species/free radicals [33].

CAT can improve the decomposition of H_2O_2 in H_2O and O_2 and is a basic ROS-scavenging enzyme. Fundamentally,

Fig. 6 Flow cytometric analysis: the percentage of viable cells (lower left and right quadrants) after the 24 h was approximately 100% for the control sample (a), 57.82% for the 30 mg/L Ag-rGO treatment (b), and 98.82% for the 30 mg/L GO treatment (c)



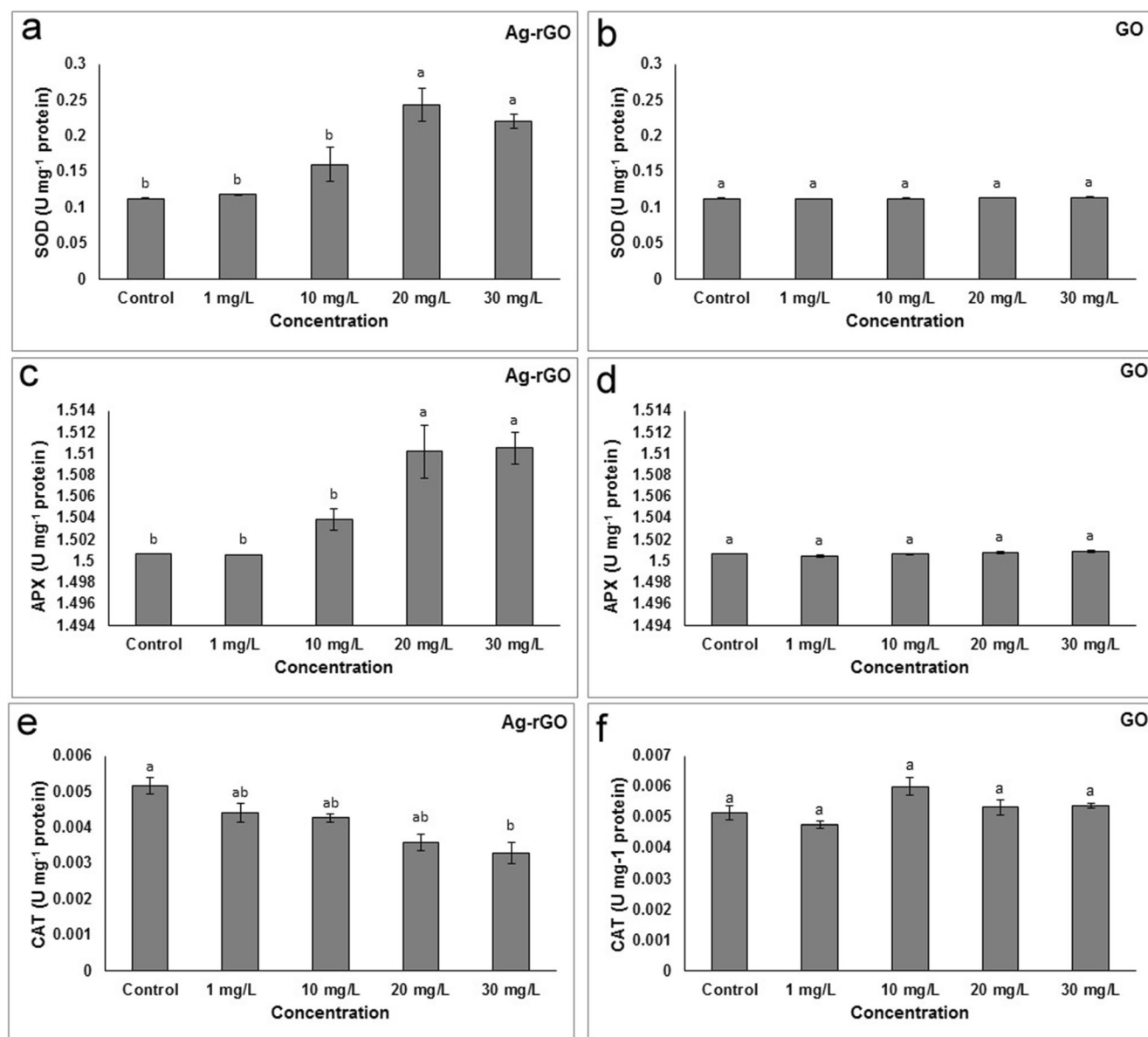


Fig. 7 SOD, APX, and CAT activities in Ag-rGO-treated (a, c, e) and GO-treated (b, d, f) *C. vulgaris* cells after 24 h of exposure. Different letters indicate significant differences at $p < 0.05$. The error bars represent standard deviation of the mean ($n = 3$ replicates)

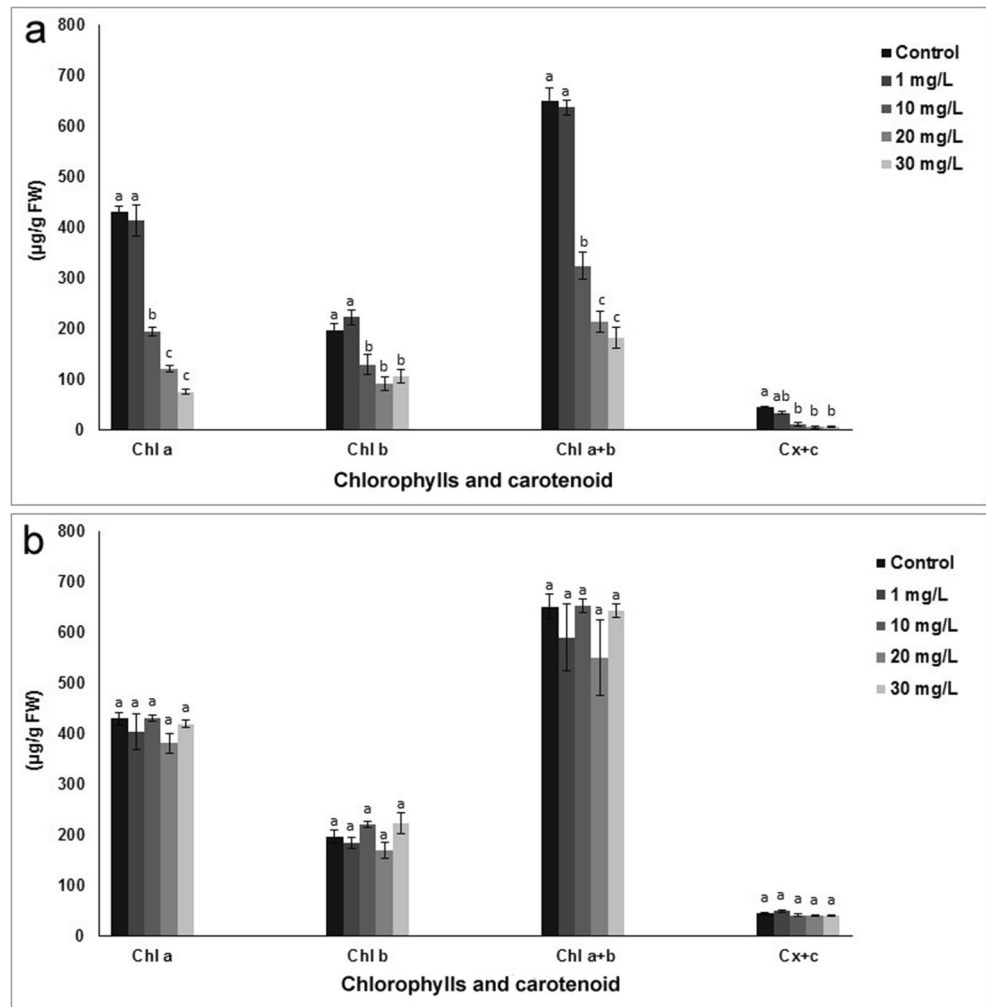
SOD/CAT way and ascorbate/glutathione cycle are both main supplementary ROS-scavenging systems [34]. Remarkably, H_2O_2 as one of the products of SOD is detoxified with CAT and APX. A statistically significant decrease in CAT activity of the cells after exposure to Ag-rGO suggests that the excess H_2O_2 was degraded by APX using ascorbate as a reductant. The reduction in CAT activity of *C. vulgaris* cells has been mentioned in the results of [31].

3.6 Photosynthetic Pigment Composition

Figure 8 shows the photosynthetic pigment content of *C. vulgaris* that were calculated using the spectrophotometric data. Treated *C. vulgaris* cells with Ag-rGO (10,

20, and 30 mg/L) displayed a significant decrease in chlorophyll and carotenoid contents after 24 h of cultivation (Fig. 8a). Ag-rGO had the highest inhibitory effect at the concentration of 30 mg/L. In contrast, at the concentration of 1 mg/L, Ag-rGO had a resembling effect on the content of photosynthetic pigments in *C. vulgaris* cells in comparison with the control. The results showed no significant difference in chlorophyll and carotenoid contents for GO treatment (Fig. 8b). The decline of chlorophyll levels of *C. vulgaris* under exogenous stress has also been previously described [35, 36]. Decrease of chlorophyll contents is one of the foremost indicators for oxidative stress [37]. The preliminary cause of photosynthetic pigment destruction can be due to the electron transport chain impairment and

Fig. 8 Effects of Ag-rGO (a) and GO (b) on the photosynthetic pigment content in *C. vulgaris* after 24 h of exposure. Different letters indicate significant differences at $p < 0.05$. The error bars represent standard deviation of the mean ($n = 3$ replicates)



substitution of Mg^{2+} ions associated with the tetrapyrrole ring of chlorophyll molecules [38].

3.7 Ag-rGO as a Potent Anti-Biofouling Agent

The buildup and growth of microorganism such as plants and algae on manmade wetted surfaces is known as biofouling and is a substantial problem especially for shipping industry [39, 40]. Numerous antifouling agents have been developed over the decades, from copper and lead sheathing to paints containing compounds of copper, lead, arsenic, and mercury in the twentieth century [41]. These products are environmentally harmful, and thus, various alternatives have been established such as fouling release coatings (e.g., polyelectrolyte multilayers (PEM) and polydimethylsiloxanes (PDMS)). These biologically benign systems are actually based on solely physical impacts [39, 42]. Considering the toxicity of Ag-rGO to *C. vulgaris* as a relatively tough marine species, this nanomaterial can be also taken into the account as a potent anti-biofouling material in the forthcoming studies.

Microtopographical and mechanical characteristics of antifouling materials such as size and roughness play an important role in preventing the attachment and growth of microorganisms on artificial surfaces [43]. For example, microtopographies with pores smaller than the cells of fouling organisms reduce their settlement and growth on the surfaces. Moreover, surface roughness defines the hydrodynamic properties of antifouling agents and affects the settlement efficiency of fouling organisms [42, 43]. According to the SEM micrographs, the produced GO and Ag-rGO are morphologically rough nanostructures. Preventing biofouling settlement via structural characteristics of Ag-rGO as a potent antifouling material is a promising issue and it might be investigated in details in future works.

4 Conclusions

The current study offered new insights on the toxic impacts of Ag-rGO to the marine microalga *C. vulgaris*. SEM images

and flow cytometric data revealed the toxicity of Ag-rGO on the algal cells. In addition, the toxicity of Ag-rGO on the algal cells was confirmed by alterations in the activity of antioxidant enzymes and reductions in growth parameters and photosynthetic pigment contents. Investigating the effects of GO on *C. vulgaris* cells at the same concentrations indicated that the toxic impacts of Ag-rGO are related to the Ag nanoparticles in the construction of these nanocomposites. As a result, this nanomaterial can be considered as a promising anti-biofouling agent in the industrial systems.

Acknowledgments The authors are indebted to R. Tarrahi for critically reading the manuscript. The authors thank the University of Tabriz, Iran, for all the support provided.

References

- Hu, X., & Zhou, Q. (2013). Health and ecosystem risks of graphene. *Chemical Reviews*, *113*(5), 3815–3835.
- Jastrzebska, A. M., Kurtycz, P., & Olszyna, A. R. (2012). Recent advances in graphene family materials toxicity investigations. *Journal of Nanoparticle Research*, *14*(12), 1–21.
- Hu, C., Wang, Q., Zhao, H., Wang, L., Guo, S., & Li, X. (2015). Ecotoxicological effects of graphene oxide on the protozoan *Euglena gracilis*. *Chemosphere*, *128*, 184–190.
- Shao, W., Liu, X., Min, H., Dong, G., Feng, Q., & Zuo, S. (2015). Preparation, characterization, and antibacterial activity of silver nanoparticle-decorated graphene oxide nanocomposite. *ACS Applied Materials & Interfaces*, *7*(12), 6966–6973.
- Zhao, S., Wang, Q., Zhao, Y., Rui, Q., & Wang, D. (2015). Toxicity and translocation of graphene oxide in *Arabidopsis thaliana*. *Environmental Toxicology and Pharmacology*, *39*(1), 145–156.
- Thu, T. V., Ko, P. J., Phuc, N. H. H., & Sandhu, A. (2013). Room-temperature synthesis and enhanced catalytic performance of silver-reduced graphene oxide nanohybrids. *Journal of Nanoparticle Research*, *15*(10), 1–13.
- Qian, H., Li, J., Sun, L., Chen, W., Sheng, G. D., Liu, W., & Fu, Z. (2009). Combined effect of copper and cadmium on *Chlorella vulgaris* growth and photosynthesis-related gene transcription. *Aquatic Toxicology*, *94*(1), 56–61.
- Chen, X., Zhu, X., Li, R., Yao, H., Lu, Z., & Yang, X. (2012). Photosynthetic toxicity and oxidative damage induced by nano-Fe₃O₄ on *Chlorella vulgaris* in aquatic environment. *Open Journal of Ecology*, *2*(01), 21–28.
- Hu, X., Lu, K., Mu, L., Kang, J., & Zhou, Q. (2014). Interactions between graphene oxide and plant cells: regulation of cell morphology, uptake, organelle damage, oxidative effects and metabolic disorders. *Carbon*, *80*, 665–676.
- Chen, T.-H., Lin, C.-Y., & Tseng, M.-C. (2011). Behavioral effects of titanium dioxide nanoparticles on larval zebrafish (*Danio rerio*). *Marine Pollution Bulletin*, *63*(5), 303–308.
- Khataee, A., Movafeghi, A., Nazari, F., Vafaei, F., Dadpour, M. R., Hanifehpour, Y., & Joo, S. W. (2014). The toxic effects of L-cysteine-capped cadmium sulfide nanoparticles on the aquatic plant *Spirodela polyrrhiza*. *Journal of Nanoparticle Research*, *16*(12), 1–10.
- Cherchi, C., & Gu, A. Z. (2010). Impact of titanium dioxide nanomaterials on nitrogen fixation rate and intracellular nitrogen storage in *Anabaena variabilis*. *Environmental Science & Technology*, *44*(21), 8302–8307.
- Sadiq, I. M., Dalai, S., Chandrasekaran, N., & Mukherjee, A. (2011). Ecotoxicity study of titania (TiO₂) NPs on two microalgae species: *Scenedesmus* sp. and *Chlorella* sp. *Ecotoxicology and Environmental Safety*, *74*(5), 1180–1187.
- Sun, X., Liu, Z., Welsher, K., Robinson, J. T., Goodwin, A., Zoric, S., & Dai, H. (2008). Nano-graphene oxide for cellular imaging and drug delivery. *Nano Research*, *1*(3), 203–212.
- Jafarirad, S., Kordi, M., & Kosari-Nasab, M. (2017). Extracellular one-pot synthesis of nanosilver using *Hyssopus officinalis* L.: a biophysical approach on bioconstituent-Ag⁺ interactions. *Inorganic and Nano-Metal Chemistry*, *47*(4), 632–638.
- Suman, T., Rajasree, S. R., & Kirubakaran, R. (2015). Evaluation of zinc oxide nanoparticles toxicity on marine algae *Chlorella vulgaris* through flow cytometric, cytotoxicity and oxidative stress analysis. *Ecotoxicology and Environmental Safety*, *113*, 23–30.
- Bradford, M. M. (1976). A rapid and sensitive method for the quantitation of microgram quantities of protein utilizing the principle of protein-dye binding. *Analytical Biochemistry*, *72*(1–2), 248–254.
- Obinger, C., Maj, M., Nicholls, P., & Loewen, P. (1997). Activity, peroxide compound formation, and heme d synthesis in *Escherichia coli* HPII catalase. *Archives of Biochemistry and Biophysics*, *342*(1), 58–67.
- Boominathan, R., & Doran, P. M. (2002). Ni-induced oxidative stress in roots of the Ni hyperaccumulator, *Alyssum bertolonii*. *New Phytologist*, *156*(2), 205–215.
- Winterbourn, C. C., McGrath, B. M., & Carrell, R. W. (1976). Reactions involving superoxide and normal and unstable haemoglobins. *Biochemical Journal*, *155*(3), 493–502.
- Sukran, D., GUNES, T., & Sivaci, R. (1998). Spectrophotometric determination of chlorophyll-a, B and total carotenoid contents of some algae species using different solvents. *Turkish Journal of Botany*, *22*(1), 13–18.
- Wang, S., Zhang, Y., Ma, H. L., Zhang, Q., Xu, W., Peng, J., Li, J., Yu, Z. Z., & Zhai, M. (2013). Ionic-liquid-assisted facile synthesis of silver nanoparticle-reduced graphene oxide hybrids by gamma irradiation. *Carbon*, *55*, 245–252.
- Fu, L., Zheng, Y., Fu, Z., Wang, A., & Cai, W. (2015). Dissolved oxygen detection by galvanic displacement-induced graphene/silver nanocomposite. *Bulletin of Materials Science*, *38*(3), 611–616.
- Gong, N., Shao, K., Feng, W., Lin, Z., Liang, C., & Sun, Y. (2011). Biototoxicity of nickel oxide nanoparticles and bio-remediation by microalgae *Chlorella vulgaris*. *Chemosphere*, *83*(4), 510–516.
- Zhou, H., Wang, X., Zhou, Y., Yao, H., & Ahmad, F. (2014). Evaluation of the toxicity of ZnO nanoparticles to *Chlorella vulgaris* by use of the chiral perturbation approach. *Analytical and Bioanalytical Chemistry*, *406*(15), 3689–3695.
- Oukarroum, A., Bras, S., Perreault, F., & Popovic, R. (2012). Inhibitory effects of silver nanoparticles in two green algae, *Chlorella vulgaris* and *Dunaliella tertiolecta*. *Ecotoxicology and Environmental Safety*, *78*, 80–85.
- Ji, J., Long, Z., & Lin, D. (2011). Toxicity of oxide nanoparticles to the green algae *Chlorella* sp. *Chemical Engineering Journal*, *170*(2), 525–530.
- Qian, H., Li, J., Pan, X., Sun, L., Lu, T., Ran, H., & Fu, Z. (2011). Combined effect of copper and cadmium on heavy metal ion bio-accumulation and antioxidant enzymes induction in *Chlorella vulgaris*. *Bulletin of Environmental Contamination and Toxicology*, *87*(5), 512–516.
- Rai, U., Singh, N., Upadhyay, A., & Verma, S. (2013). Chromate tolerance and accumulation in *Chlorella vulgaris* L.: role of antioxidant enzymes and biochemical changes in detoxification of metals. *Bioresource Technology*, *136*, 604–609.
- Wang, H. Y., Zeng, X. B., Guo, S. Y., & Li, Z. T. (2008). Effects of magnetic field on the antioxidant defense system of recirculation-cultured *Chlorella vulgaris*. *Bioelectromagnetics*, *29*(1), 39–46.

31. Mallick, N. (2004). Copper-induced oxidative stress in the chlorophycean microalga *Chlorella vulgaris*: response of the antioxidant system. *Journal of Plant Physiology*, *161*(5), 591–597.
32. Chongpraditnun, P., Mori, S., & Chino, M. (1992). Excess copper induces a cytosolic Cu, Zn-superoxide dismutase in soybean root. *Plant and Cell Physiology*, *33*(3), 239–244.
33. Gupta, D., Nicoloso, F., Schetinger, M., Rossato, L., Pereira, L., Castro, G., Srivastava, S., & Tripathi, R. (2009). Antioxidant defense mechanism in hydroponically grown *Zea mays* seedlings under moderate lead stress. *Journal of Hazardous Materials*, *172*(1), 479–484.
34. Dazy, M., Masfaraud, J.-F., & Ferard, J.-F. (2009). Induction of oxidative stress biomarkers associated with heavy metal stress in *Fontinalis antipyretica* Hedw. *Chemosphere*, *75*(3), 297–302.
35. Qian, H., Chen, W., Li, J., Wang, J., Zhou, Z., Liu, W., & Fu, Z. (2009). The effect of exogenous nitric oxide on alleviating herbicide damage in *Chlorella vulgaris*. *Aquatic Toxicology*, *92*(4), 250–257.
36. Gao, Q., & Tam, N. (2011). Growth, photosynthesis and antioxidant responses of two microalgal species, *Chlorella vulgaris* and *Selenastrum capricornutum*, to nonylphenol stress. *Chemosphere*, *82*(3), 346–354.
37. di Toppi, L. S., Musetti, R., Marabottini, R., Corradi, M. G., Vattuone, Z., Favali, M. A., & Badiani, M. (2004). Responses of *Xanthoria parietina* thalli to environmentally relevant concentrations of hexavalent chromium. *Functional Plant Biology*, *31*(4), 329–338.
38. Assche, F. V., & Clijsters, H. (1990). Effects of metals on enzyme activity in plants. *Plant, Cell & Environment*, *13*(3), 195–206.
39. Frueh, J., Gai, M., Yang, Z., & He, Q. (2014). Influence of poly-electrolyte multilayer coating on the degree and type of biofouling in freshwater environment. *Journal of Nanoscience and Nanotechnology*, *14*(6), 4341–4350.
40. Cooper, S. P., Finlay, J. A., Cone, G., Callow, M. E., Callow, J. A., & Brennan, A. B. (2011). Engineered antifouling microtopographies: kinetic analysis of the attachment of zoospores of the green alga *Ulva* to silicone elastomers. *Biofouling*, *27*(8), 881–892.
41. Voulvoulis, N., Scrimshaw, M., & Lester, J. (1999). Alternative antifouling biocides. *Applied Organometallic Chemistry*, *13*(3), 135–143.
42. Chaudhury, M. K., Finlay, J. A., Chung, J. Y., Callow, M. E., & Callow, J. A. (2005). The influence of elastic modulus and thickness on the release of the soft-fouling green alga *Ulva linza* (syn. *Enteromorpha linza*) from poly (dimethylsiloxane) (PDMS) model networks. *Biofouling*, *21*(1), 41–48.
43. Xiao, L., Thompson, S. E., Rohrig, M., Callow, M. E., Callow, J. A., Grunze, M., & Rosenhahn, A. (2013). Hot embossed microtopographic gradients reveal morphological cues that guide the settlement of zoospores. *Langmuir*, *29*(4), 1093–1099.